Analyzing the bistability of the minimally bistable ERK network using the discriminant locus

Daniel Hwang

April 18th, 2022

Abstract

The extracurricular signal regulated kinase (ERK) system is a biological signaling network with "important roles in regulating cellular activity" [1]. For this project, we will analyze the bistability, i.e, its capacity to hold two or more positive steady states that are stable to small perturbations [2], of the minimally bistable ERK network by analyzing its number of real positive steady states for different parameterizations of the network. Previous research used mixed volume computations to determine that the possible range of positive steady states is 1 to 5 [1], however, it has been conjectured that the maximum number of positive steady states is 3 [3]. While this system has been analyzed from a convex geometry perspective [1], our goal is to analyze the ERK system from an algebraic perspective by generalizing the behavior of the steady states of the ERK system over a two-dimensional parameter space in terms of parameters $\{k_{\text{cat}}, k_{\text{on}}\}$, which primarily impact bistability. We use homotopy continuation to discretely sample the discriminant locus and inflection curves of the parameter space, which separates the parameter space into distinct regions each corresponding to a constant number of positive real solutions. Our results demonstrate that in two different parameterizations of the network that the maximum number of positive steady states was 3 and that the relationship between the rate constants was the primary factor in determining this upper bound.

1 Introduction

The extracurricular signal regulated kinase (ERK) system is a biological signaling network with "important roles in regulating cellular activity" [1], some of which include "proliferation, differentiation, development, and under certain conditions cell survival" [4]. This functionality extends further to humans, for whom ERK activity is present in the neurological areas that contribute to learning and memory [5], and abnormal ERK activity contributes to feelings of pain and depression [6, 7]. Understanding how the ERK system functions and how to control its activity would lead to more effective treatment of pain and promote healthy cell regulation by directing signals to appropriate destinations. To further understand how the ERK system processes and encodes stimuli, we investigate the bistability of the ERK system, i.e, whether it has the capacity to hold two or more positive steady states that are stable to small perturbations [2]. We define the positive steady states of the ERK system to be positive combinations of all chemical species such that the system experiences no change. Evidence that the ERK system is bistable would imply that it behaves as a biological switch or clock [8]. For this project, we investigate whether the ERK system, specifically, the minimally bistable ERK subnetwork, is bistable by analyzing its number of positive steady states for varying parameter values.

The minimally bistable ERK subnetwork is generated by making all reactions in the ERK network irreversible by removing the two-way reactions in the original ERK network shown in Figure 1, since irreversibility does not impact bistability [3].

After removing the two-way reactions, we can now describe the minimally bistable ERK subnetwork: let $x_1, \ldots, x_{12}$ denote the concentrations of their respective species listed in Table 1. The concentrations obey the following ODE system:

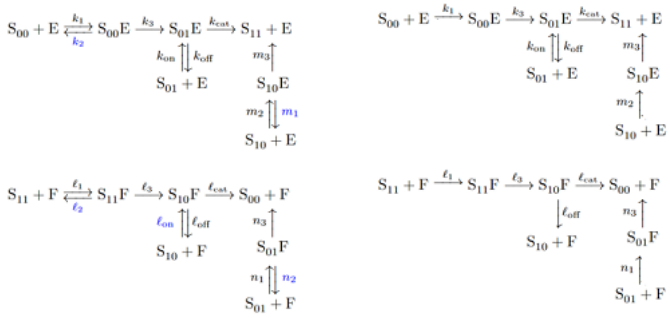

(a) (b)

Figure 1: (a) The original ERK network. (b) The minimally bistable ERK network generated by removing the reactions $k_2, m_1, l_2, l_{\text{on}}, n_2$ (marked as blue on (a)).

x_1	x_2	x_3	x_4	x_5	x_6	x_7	x_8	x_9	x_{10}	x_{11}	x_{12}
S_{00}	E	F	$S_{11}F$	$S_{10}F$	$S_{01}F$	$S_{01}E$	$S_{10}E$	S_{01}	S_{10}	$S_{00}E$	S_{11}

Table 1: Assignment of variables to chemical species for the minimally bistable ERK network.

$$\dot{x}_1 = -k_1x_1x_2 + \ell_{\text{cat}}x_5 + n_3x_6 \tag{1}$$
$$\dot{x}_2 = -k_1x_1x_2 - k_{\text{on}}x_2x_9 - m_2x_{10}x_2 + k_{\text{cat}}x_7 + k_{\text{off}}x_7 + m_3x_8 \tag{2}$$
$$\dot{x}_3 = -\ell_1x_3x_{12} - n_1x_3x_9 + \ell_{\text{cat}}x_5 + \ell_{\text{off}}x_5 + n_3x_6 \tag{3}$$
$$\dot{x}_4 = \ell_1x_3x_{12} - \ell_3x_4 \tag{4}$$
$$\dot{x}_5 = \ell_3x_4 - \ell_{\text{cat}}x_5 - \ell_{\text{off}}x_5 \tag{5}$$
$$\dot{x}_6 = n_1x_3x_9 - n_3x_6 \tag{6}$$
$$\dot{x}_7 = k_{\text{on}}x_2x_9 + k_3x_{11} - k_{\text{cat}}x_7 - k_{\text{off}}x_7 \tag{7}$$
$$\dot{x}_8 = m_2x_2x_{10} - m_3x_8 \tag{8}$$
$$\dot{x}_9 = -k_{\text{on}}x_2x_9 - n_1x_3x_9 + k_{\text{off}}x_7 \tag{9}$$
$$\dot{x}_{10} = -m_2x_2x_{10} + \ell_{\text{off}}x_5 \tag{10}$$
$$\dot{x}_{11} = k_1x_1x_2 - k_3x_{11} \tag{11}$$
$$\dot{x}_{12} = -\ell_1x_3x_{12} + k_{\text{cat}}x_7 + m_3x_8 \tag{12}$$

where $\kappa = (k_1, k_3, k_{\text{cat}}, k_{\text{on}}, k_{\text{off}}, \ell_1, \ell_3, \ell_{\text{cat}}, \ell_{\text{off}}, m_2, m_3, n_1, n_3)$ is the rate-constant vector that parameterizes the above ERK system [3]. In addition, the ERK system must obey the following conservation equations corresponding to the total amounts of substrate S, kinase E, and phosphatase F respectively:

$$x_1 + x_4 + x_5 + x_6 + x_7 + x_8 + x_9 + x_{10} + x_{11} + x_{12} = S_{\text{tot}} = c_1 \tag{13}$$
$$x_2 + x_7 + x_8 + x_{11} = E_{\text{tot}} = c_2 \tag{14}$$
$$x_3 + x_4 + x_5 + x_6 = F_{\text{tot}} = c_3 \tag{15}$$

The parameters k_{on} and k_{cat} are primary in determining the bistability of this ERK subnetwork [3]. With that as the focus, we fix all parameters in κ and $\{c_1, c_2, c_3\}$ at 1 except for $\{k_{\text{cat}}, k_{\text{on}}\}$ and our goal becomes to analyze the number of positive steady states for different combinations of $\{k_{\text{cat}}, k_{\text{on}}\}$.

For a given steady state of the minimally bistable ERK subnetwork, the change in chemical concentration is 0 for each species in the system, therefore, to solve for the steady states, we solve for the real solutions to $\dot{x}_1, \ldots, \dot{x}_{12} = 0$. Additionally, since our steady states must satisfy the conservation equations, we impose

the additional equations $S_{\text{tot}} - c_1 = 0, E_{\text{tot}} - c_2 = 0, F_{\text{tot}} - c_3 = 0$. Thus, solving this polynomial system of 15 equations in 12 variables and parameters $\{k_{\text{cat}}, k_{\text{on}}\}$ will yield steady states to the system, given the other 11 rate constants are fixed at constant values. Since the system has 3 equations that are dependent on the others, the number of equations we solve for becomes 12, turning our polynomial system into a square system with a finite number of solutions.

Previous research used mixed volume computations to determine that the possible range of positive steady states is 1 to 5 [1]. However, Conjecture 6.2 of [3] asserts that the maximum number of positive steady states is 3. While this system has been analyzed from a convex geometry perspective, our goal is to analyze the ERK system from an algebraic perspective by generalizing the behavior of the steady states of the ERK system over a two-dimensional parameter space and then certifying the numerical results to confirm the conjecture. Specifically, we discretely compute the discriminant locus of the given polynomial system to separate the parameter space into distinct regions based on the number of real solutions. In order to do this, we compute pseudo-witness set points on the discriminant locus via homotopy continuation.

We begin by providing a brief background on homotopy continuation in Section 2, which will be used to numerically track the solutions for a parameterized polynomial system from a generic polynomial start system. This technique is imperative to analyzing the parameter space by sampling the pseudo-witness set points on its discriminant locus in Section 3. We will also use homotopy continuation to discretely compute inflection curves that further separate the parameter space into regions containing the same sign of each of the variables x_i and thus containing the same number of positive, real steady states. Finally, we discuss the numerical results and their impact on the number of (positive) real solutions of the minimally bistable ERK subnetwork in Sections 4 and 5.

2 Background on homotopy continuation

We are interested in the solutions to square parameterized polynomial systems of the form

$$F(x;p) = \begin{bmatrix} F_1(x_1, \ldots, x_n; p_1, \ldots, p_k) \\ \vdots \\ F_n(x_1, \ldots, x_n; p_1, \ldots, p_k) \end{bmatrix} = 0 \tag{16}$$

where $F_1(x;p), \ldots, F_n(x;p)$ are polynomials with complex coefficients within our square parameterized polynomial system $F(x;p)$ [9]. Moreover, since F is square, we assume F is 0-dimensional and the solution set $\mathbb{V}(F)$ is finite. We also assume that these solutions x^* are nonsingular, i.e, $J_x F(x^*;p)$, the Jacobian matrix of F with respect to x, is invertible at each x^*. These assumptions are made to ensure that when we numerically compute the solutions to F, the solutions will be well-behaved at each time-step. We will solve for the solutions to $F(x;p)$ for any fixed parameter p in two phases: the ab initio phase and parameter homotopy phase.

2.1 Ab initio phase

In the ab initio phase, our goal is to solve for the solutions to our target system $F(x;p_0)$ for some random parameter $p_0 \in \mathbb{C}^k$. In order to achieve this, we construct a similar start system $G(x)$ whose solutions we know. This start system is often defined as

$$G(x) = \begin{bmatrix} x_1^{d_1} - 1 \\ \vdots \\ x_n^{d_n} - 1 \end{bmatrix} \tag{17}$$

where d_i is the respective degree of each polynomial F_i as defined in (16) [10]. Now, we can construct a total-degree homotopy H defined as a continuous map

$$H : [0,1] \times \mathbb{C}^n \to \mathbb{C}^n$$

such that $H(1,x) = G(x)$ and $H(0,x) = F(x;p_0)$. One such example of a total-degree homotopy is

$$H(t,x) = t * G(x) + (1-t) * F(x;p_0) \tag{18}$$

that satisfies $H(1,x) = G(x)$ and $H(0,x) = F(x;p_0)$. If the equation $H(t,x) = 0$ has a unique root for each $t \in [0,1]$, then that root is a function of t, and we can write $x(t)$ as the unique member of $\mathbb{C}^n$ such that $H(t,x(t)) = 0$, and we can view $[x(t) : 0 \leq t \leq 1]$ as an arc in $\mathbb{C}^n$ parameterized by t, starting at a known solution to $G(x)$ at $t = 1$ and moving towards a solution to $F(x;p_0)$ at $t = 0$ [11]. Repeating this process for all known solutions to $G(x)$ yields all solutions to $F(x;p_0)$ using this method. While we track all paths, we will consider only the nonsingular isolated solutions to $F(x;p_0)$. The details for path tracking are explained in Appendix A.

For our purposes, we will utilize the "gamma-trick" homotopy [12], which uses a random $\gamma \in \mathbb{C}$ with $|\gamma| = 1$ to construct the following homotopy:

$$H(t,x) = \gamma t * G(x) + (1-t) * F(x;p_0) \tag{19}$$

Note that the gamma-trick homotopy to change the paths from $t = 1$ to $t = 0$ on $\mathbb{R}^n$ to curves on $\mathbb{C}^n$, making the path generic for t in $(0,1]$ with probability 1 and thus, avoiding any singularities.

2.2 Parameter homotopy phase

Now that we've solved for the solutions to $F(x;p_0)$, we can use a parameter homotopy to track the solutions from $F(x;p_0)$ to $F(x;p)$ for $p \in \mathbb{C}^n$:

$$H(t,x) = F(x; t * p_0 + (1-t) * p). \tag{20}$$

Observe that $H(1,x) = F(x;p_0)$ and $H(0,x) = F(x;p)$. Therefore, if we can track the possible paths $[x(t); 0 \leq t \leq 1]$ starting at each of the nonsingular isolated solutions to $F(x;p_0)$ at $t = 1$, we can compute the set of solutions to $F(x;p)$ at $t = 0$.

We utilize this approach because for many applications, solving quickly for the solutions at many different parameter values is desired. A parameter homotopy allows for the efficient and accurate solving at many instances of the parameters by focusing only on the nonsingular isolated solutions to the system.

3 Sampling the discriminant locus

We observe from past literature [9] that for any real polynomial system F, the discriminant locus is the set of all points $p \in \mathbb{C}^k$ where there exists a solution x to $F(x;p) = 0$ and $\det(J_x(F(x;p))) = 0$, where $J_x(F(x;p))$ is the Jacobian matrix of F. The discriminant locus is particularly useful because it separates the parameter space into distinct regions containing the same number of real solutions [9].

As an example, consider the number of real solutions for a monic quadratic $x^2 + bx + c$ and a monic cubic $x^3 + bx + c$ over the parameter space $[-1,1] \times [-1,1]$ as in Figure 2 [9]. The white points represent the discretely computed points of the discriminant locus. These points satisfy $D = 0$, where D is each polynomial's respective discriminant. We observe that as we "cross" the discriminant locus, the number of real solutions to F changes by 2. Solutions to a polynomial with real coefficients must either be real or be part of a complex conjugate pair. Moreover, whenever we cross the discriminant locus, we either add or remove a complex conjugate pair, changing the number of real solutions by 2.

We can discretely compute the discriminant locus by repeatedly "slicing" the parameter space, as demonstrated in Figure 3 [9]. In Figure 3, we take linear slices of the parameter space by fixing the parameter b (on the x-axis of the figure) to be equal to some constant value and found the solutions $(x;p)$ to $F(x;p) = 0$ and $\det(J_x(F(x;p)) = 0$. We call the set of points p from these solutions the pseudo-witness set points [9]. By repeating this process for different lines as shown in Figure 3, we are able to discretely compute the discriminant locus. Utilizing the parameter homotopy method, we can quickly complete multiple runs using the solutions from an ab initio phase (computing the solutions to $F(x;p_0)$ for random p_0) and tracking them to the solutions of $F(x;p)$, where $p \in \mathbb{C}^n$.

Applying this method to our polynomial system described by (1), we solve for solutions $(x;p)$ to the following system:

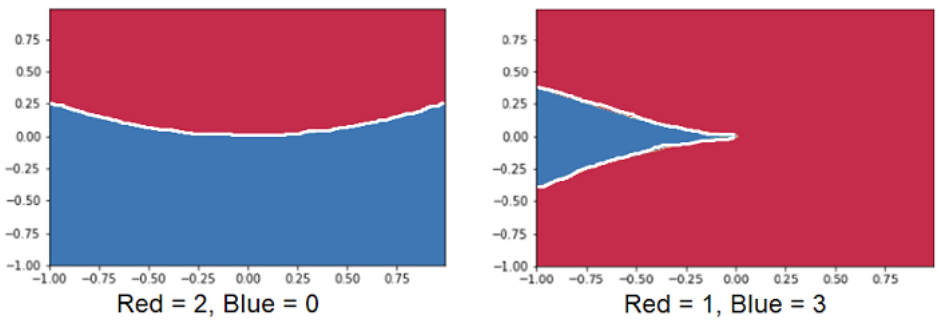

(a) (b)

Figure 2: The number of real solutions to (a) the quadratic $x^2 + bx + c$ and (b) the cubic $x^3 + bx + c$ over the parameter space $(b, c) \in [-1, 1] \times [-1, 1]$.

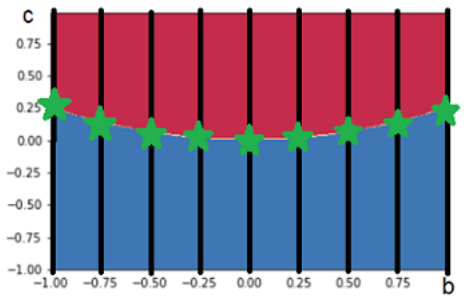

Figure 3: The pseudo-witness set points (green stars) calculated by slicing the discriminant locus across lines of the form $b = \alpha$.

$$F(x; p) = 0 \tag{21}$$

$$\det(J_x(F(x; p))) = 0 \tag{22}$$

$$(k_{\text{cat}} - \alpha) \text{ OR } (k_{\text{on}} - \alpha) = 0 \tag{23}$$

for parameter α, where

$$F(x; p) = \begin{pmatrix} \dot{x}_1 \\ \vdots \\ \dot{x}_{12} \\ S_{\text{tot}} - c_1 \\ E_{\text{tot}} - c_2 \\ F_{\text{tot}} - c_3 \end{pmatrix} \tag{24}$$

Here, α is the value at which we fix k_{on} or k_{cat}, allowing us to "slice" the discriminant locus by finding its intersections with the $k_{\text{on}} = \alpha$ or $k_{\text{cat}} = \alpha$ for different values of α.

3.1 Positivity

In addition to determining which regions of the parameter space contain the same number of real solutions, our goal is to investigate the positivity of the real solutions within these regions. Similar to how we computed the discriminant locus, we can detect where the positivity of the solution set changes by computing the

inflection points of each component x_i in x. Moreover, we solve for the set of parameter values where $x_i = 0$ for $i \in \{1, \ldots, 12\}$. This means if we modify the system in (21) to be

$$F(x; p) = 0 \tag{25}$$

$$x_i = 0 \tag{26}$$

$$(k_{\text{cat}} - \alpha) \text{ OR } (k_{\text{on}} - \alpha) = 0 \tag{27}$$

for all $i \in \{1, \ldots, 12\}$, then we can discretely compute the set of points over the parameter space for which there is a change in positivity, which separates the complement of this set into distinct regions containing solutions with the same positivity. Overlaying this graph on top of our existing discriminant locus allows us to separate the parameter space into regions containing the same number of positive real solutions.

4 Results

This section describes the results from discretely sampling the discriminant locus by solving the system beginning at (21). While initially the system seems overdetermined, there is a dependence relation between various equations that can allow us to reduce the total number of equations to 12 - thus yielding a square system. Having a square system removes any numerical instability that could impact the accuracy of the homotopy continuation computations. We found the following linear dependencies:

$$\dot{x}_2 + \dot{x}_7 + \dot{x}_8 + \dot{x}_{11} = 0 \tag{28}$$

$$\dot{x}_3 + \dot{x}_4 + \dot{x}_5 + \dot{x}_6 = 0 \tag{29}$$

$$\dot{x}_1 + \dot{x}_4 + \dot{x}_5 + \dot{x}_6 + \dot{x}_7 + \dot{x}_8 + \dot{x}_9 + \dot{x}_{10} + \dot{x}_{11} + \dot{x}_{12} = 0 \tag{30}$$

After removing equations $\dot{x}_1, \dot{x}_2, \dot{x}_3$ from $F(x; p)$, we implemented homotopy continuation to generate the set of pseudo-witness set points as described in Section 3.

4.1 All-1 case

We started with a simple case where all values in parameter vector κ except for k_{cat} and k_{on} were fixed to be 1. We sampled the pseudo-witness set points by finding their intersections with linear slices of the parameter space of the form $k_{\text{cat}} = \alpha$ and $k_{\text{on}} = \alpha$ where α was sampled from the interval $[0.1, 150]$ with a 0.1 step size between adjacent points. In addition, we took linear slices of the form $k_{\text{cat}} = \alpha$ with a 0.01 step size on the interval $[0.1, 5]$ and $k_{\text{on}} = \alpha$ with a 0.01 step size on the interval $[0.1, 2.5]$ to capture smaller regions of the parameter space, as observed in Figure 4.

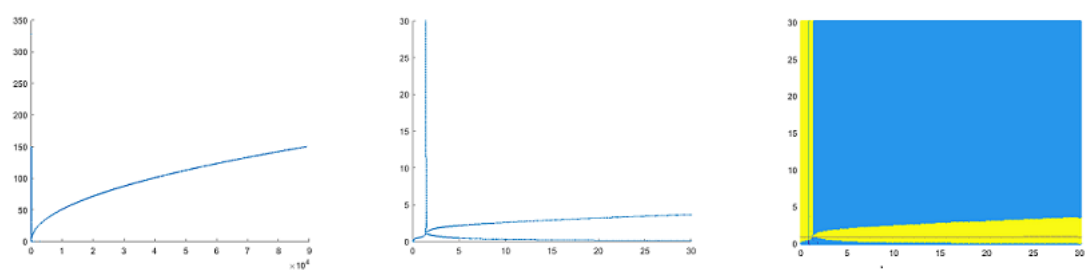

(a) (b) (c)

Figure 4: (a) The set of sampled pseudo-witness set points for $F(x; p)$ found by linear slices in the regions of $k_{\text{cat}} = [0, 150]$, $k_{\text{on}} = [0, 150]$, (b) the same set of sampled points falling within the region $k_{\text{cat}} = [0, 30], k_{\text{on}} = [0, 30]$, and (c) the number of real solutions over the region $k_{\text{cat}} = [0, 30]$, $k_{\text{on}} = [0, 30]$. The blue regions contain 3 real solutions, while the yellow regions contain 5 real solutions.

The left and middle parts of Figure 4 show the pseudo-witness set points of the ERK network calculated, with the left part showing all sampled points and the middle part showing the set of points within the region

$k_{\text{cat}} = [0, 30]$ and $k_{\text{on}} = [0, 30]$ of the parameter space. We observe that in both sides, the discretely calculated discriminant locus splits the majority of the parameter space into two separate regions on the right. We also observe that the middle and right parts of Figure 4 respectively show the set of pseudo-witness set points of the discriminant locus on the middle and the number of real solutions on the right, both sampled over the region $k_{\text{cat}} = [0, 30]$ and $k_{\text{on}} = [0, 30]$ of the parameter space with a step size 0.1 along these intervals. Note that the blue regions contain 3 real solutions, while the yellow regions contain 5 real solutions.

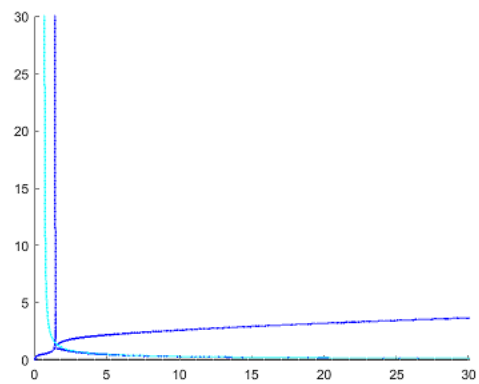

Figure 5: The inflection curves (light blue) mapped over the existing discriminant locus (dark blue) from Figure 4 over the region $k_{\text{cat}} = [0, 30], k_{\text{on}} = [0, 30]$.

Figure 5 shows the parameter space after overlaying the inflection curves described in Section 3.1 on the existing discriminant locus on Figure 4. We then checked each region and confirmed the number of positive real solutions in every region across the parameter space is 1.

4.2 Parameterized case

These initial results provided strong evidence that the choices of k_{cat} and k_{on} did not have an impact on the number of positive real solutions, despite the change in the number of real solutions. We decided to investigate the following parameterization [1] of the rate constants that achieves 3 positive steady states in certain cases:

$$(k_1, k_3, k_{\text{cat}}, k_{\text{on}}, k_{\text{off}}, \ell_1, \ell_3, \ell_{\text{cat}}, \ell_{\text{off}}, m_2, m_3, n_1, n_3) = (\frac{1}{t}, \frac{1}{t}, k_{\text{cat}}, k_{\text{on}}, 1, t, \frac{1}{t}, 1, 1, 1, 1, 1, 1) \tag{31}$$

with constants

$$c_1 = \frac{3k_{\text{cat}}k_{\text{on}}t^3 + 3k_{\text{cat}}k_{\text{on}}t^2 + 3k_{\text{cat}}k_{\text{on}}t + 3t^2k_{\text{cat}} + k_{\text{on}}t^2 + 3tk_{\text{cat}} + t^2 + 3k_{\text{cat}} + 4t}{k_{\text{cat}}k_{\text{on}}t + k_{\text{cat}} + 1} \tag{32}$$

$$c_2 = \frac{t(k_{\text{cat}}k_{\text{on}}t^2 + 2k_{\text{cat}}k_{\text{on}}t + tk_{\text{cat}} + k_{\text{on}}t + 2k_{\text{cat}} + t + 2)}{k_{\text{cat}}k_{\text{on}}t + k_{\text{cat}} + 1} \tag{33}$$

$$c_3 = \frac{2k_{\text{cat}}k_{\text{on}}t^3 + k_{\text{cat}}k_{\text{on}}t^2 + k_{\text{cat}}k_{\text{on}}t + 2t^2k_{\text{cat}} + tk_{\text{cat}} + k_{\text{cat}} + t + 1}{k_{\text{cat}}k_{\text{on}}t + k_{\text{cat}} + 1} \tag{34}$$

for $t > 0$. Let the numerators of each of these constants be u_1, u_2, u_3.

In order to make this system of equations into a polynomial system, we multiplied both sides of the conservation equations by $(k_{\text{cat}}k_{\text{on}}t + k_{\text{cat}} + 1)$ so that the system of equations (24) became:

[1] This parameterization was provided to us by Dr. Nida Obatake of University of California, San Diego; Institute of Defense Analysis

$$F(x;p) = \begin{pmatrix} \dot{x}_1 \\ \vdots \\ \dot{x}_{12} \\ (k_{\text{cat}}k_{\text{on}}t + k_{\text{cat}} + 1)S_{\text{tot}} - u_1 \\ (k_{\text{cat}}k_{\text{on}}t + k_{\text{cat}} + 1)E_{\text{tot}} - u_2 \\ (k_{\text{cat}}k_{\text{on}}t + k_{\text{cat}} + 1)F_{\text{tot}} - u_3 \end{pmatrix} \tag{35}$$

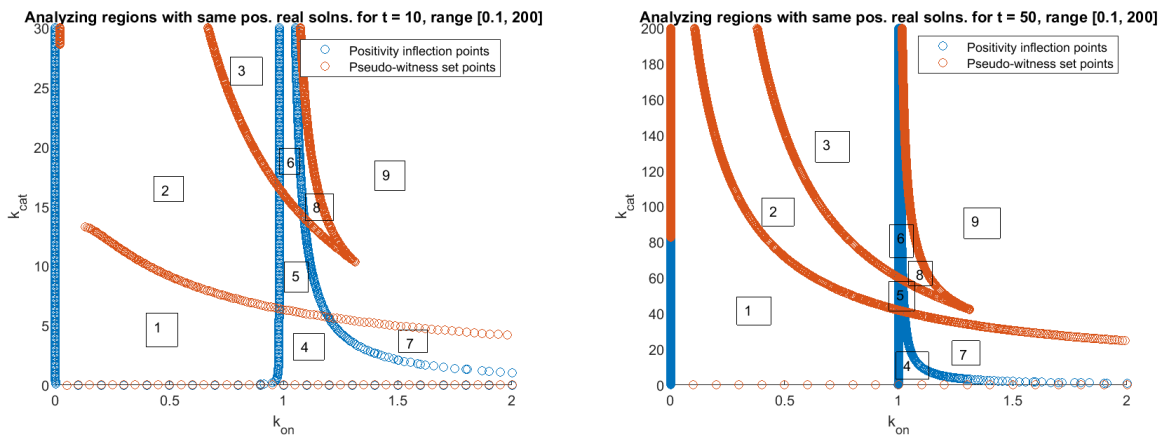

(a) (b)

Figure 6: (a) The inflection curves (dark blue) mapped over the existing discriminant locus curves (orange) over the region $k_{\text{cat}} = [0, 2], k_{\text{on}} = [0, 30]$ for the $t = 10$ system and (b) the region $k_{\text{cat}} = [0, 2], k_{\text{on}} = [0, 200]$ for the $t = 50$ system.

We sampled the discriminant locus for the above parameterized system for $t = 10$ and $t = 50$ over the intervals $k_{\text{cat}} = [0.1, 200]$ and $k_{\text{on}} = [0.1, 200]$, along with the inflection curves in Figure 6. We then tested for the number of real solutions and the number of positive real solutions in each of these regions in Table 2. In Figure 6, regions 1, 4, and 7 of the parameter space on the left hand side (t = 10) and on the right hand side (t = 50) resulted in 3 positive real solutions. In both cases, these regions of the parameter space corresponding to 3 positive real solutions formed the component of the discriminant locus curve closest to the k_{on} axis.

Region	Real	# Pos. Real
1	5	3
2	3	1
3	5	1
4	5	3
5	3	1
6	5	1
7	5	3
8	5	1
9	3	1

Table 2: The number of real solutions and the number of positive real solutions in each of the regions in Figure 6 for the $t = 10$ and $t = 50$ systems.

5 Discussion and future work

The main challenge with testing the parameterized system described in Section 4.2 was that as t increased, the coefficient bound increased. In particular, the coefficients for the determinant equation in (21) became dependent on t^3 and $\frac{1}{t^3}$, which made it difficult to track the solutions to this system as t increases. In particular, as $\frac{1}{t^3}$ converges towards 0, the terms in the equation with a $\frac{1}{t^3}$ also converge towards 0, which effectively removes these terms from the equation and alters the numerical solutions to this system. Additionally, having this spread of coefficients from t^3 to $\frac{1}{t^3}$ doesn't allow for the implementation of a scale factor to control the stability of the numerical methods. This phenomena occurred of values of $t \geq 100$, yielding zero nonsingular isolated solutions to the parameterized polynomial system, and thus, not allowing for any analysis of the parameter space.

Moreover, the degree of the determinant equation in the parameterized system was 13, which drastically increased the complexity of the polynomial system and moreover, the runtime of the parameter homotopy. This was resolved by enabling regeneration [12], where instead of tracking the solutions to the start system G to the solutions of all the equations in the target system F, we incrementally solve for the solutions from the intermediate start system $G_i = \{f_1, \ldots, f_{i-1}, g_i, l_{i+1}, \ldots, l_N\}$ to the intermediate target system $F_i = \{f_1, \ldots, f_{i-1}, f_i, l_{i+1}, \ldots, l_N\}$ where l_i are general linear equations. By carrying over the solutions from F_{i-1} to F_i, we reduce the number of solutions to consider at each phase and significantly decrease the runtime of the program. However, for $t \geq 100$, we were unable to generate finite solutions for the parameterized polynomial system, suggesting that this numerical approach to this problem is ineffective for high values of $t \geq 100$.

The results presented in the reciprocal case in Section 4.2 support Conjecture 6.2 of [3] that the maximum number of positive steady states is 3. Moreover, these results support the claim there exists at least one parameterization for which 3 positive steady states can be achieved and thus at least one parameterization for which 3 positive steady states can be achieved and thus at least one parameterization where the ERK system is bistable.

Contrary to our original hypothesis that the choice of the parameters $k_{\text{cat}}, k_{\text{on}}$ is the primary factor in determining the bistability of the ERK network, we conclude the relationship between the rate constants primarily controls the number of positive steady states of the ERK network. It appears the relationship between the parameters impacted which values of $k_{\text{cat}}, k_{\text{on}}$ resulted in pseudo-witness set points. Moreover, the region of 3 positive real solutions contained solutions where k_{cat} and k_{on} were close to 0, implying that the actual values of k_{cat} and k_{on} does not matter as much compared to the relationship of the other parameters.

To account for positivity, we also sampled the inflection curves associated with each system as defined in Section 3.1. However, the results from the above case, in addition to the sample all-1 case in Section 4.1, show that these curves do not impact the number of positive real solutions. Rather, any change, if present, in the number of positive real solutions across different regions of the parameter space only occurred if those regions were separated by the discriminant locus.

In the future, we want to first confirm there exists no other value of t for our current parameterization that yields 5 steady states by testing low values of t such as $\frac{1}{50}$ and see if the discriminant locus and positivity inflection curves maintain their current structure. We wish to also observe the number of positive steady states for other parameterizations of the ERK system that potentially allow us to achieve 3 or more positive steady states in order to prove or disprove the conjecture. Finally, we wish to investigate the relationship between the rate constants and their impact on the number of positive steady states to gain a further understanding of how the ERK system behaves and how it reacts to different parameterizations.

6 Acknowledgements

The author would like to thank Dr. Maggie Regan for her invaluable feedback, constant support, and excellent advising over this project, Dr. Nida Obatake at University of California, San Diego; Institute for Defense Analysis for collaborating with us and providing the parameterization in Section 4.2, and Dr. David Kraines for running the PRUV program. All code and figures were generated using MATLAB (https://mathworks.com). We utilized the homotopy continuation software Bertini (https://bertini.nd.edu) to numerically implement the path-tracking.

References

[1] Nida Obatake et al. "Oscillations and bistability in a model of ERK regulation" (2019). arXiv: 1903.02617 [q-bio.MN].

[2] Carsten Conradi and Anne Shiu. "Dynamics of Posttranslational Modification Systems: Recent Progress and Future Directions". *Biophysical jounral* 114 (2018), pp. 507–515. DOI: doi:10.1016/j.bpj.2017.11.3787.

[3] Carsten Conradi et al. "Dynamics of ERK regulation in the processive limit" (2020). arXiv: 1910.14452 [q-bio.MN].

[4] Yoav D. Shaul and Rony Seger. "The MEK/ERK cascade: from signaling specificity to diverse functions". *Biochimica et biophysica acta* 1773 (2007), pp. 1213–26. DOI: 10.1016/j.bbamcr.2006.10.005.

[5] S. Blum and P.K. Dash. "MAP Kinase Signaling in Learning and Memory" (2009), pp. 657–662. DOI: https://doi.org/10.1016/B978-008045046-9.00821-4.

[6] Célia D Cruz and Francisco Cruz. "The ERK 1 and 2 pathway in the nervous system: from basic aspects to possible clinical applications in pain and visceral dysfunction". *Current neuropharmacology* 5,4 (2007), pp. 244–52. DOI: 10.2174/157015907782793630.

[7] J.Q Wang and L. Mao. "The ERK Pathway: Molecular Mechanisms and Treatment of Depression". *Molecular neurobiology* 56,9 (2019), pp. 6197–6205. DOI: 10.1007/s12035-019-1524-3.

[8] John J Tyson et al. "Biological switches and clocks". *Journal of the Royal Society, Interface* 5 Suppl 1 (2008), S1—8. ISSN: 1742-5689. DOI: 10.1098/rsif.2008.0179.focus.

[9] Edgar A. Bernal et al. "Machine learning the real discriminant locus" (2020). arXiv: 2006.14078 [stat.ML].

[10] Anton Leykin. *Introduction to Algebraic Computation Notes*. 2013, pp. 13–27. URL: https://antonleykin.math.gatech.edu/math4803spr13/BOOK/chapter2.pdf.

[11] David Kincaid and Ward Cheney. *Numerical Mathematics and Computing, 5th Edition*. Brooks/Cole Publishing Company, 2004. ISBN: 0-534-38993-7. URL: https://web.ma.utexas.edu/CNA/NMC5/.

[12] Daniel J. Bates et al. *Numerically Solving Polynomial Systems with Bertini*. Society for Industrial and Applied Mathematics, 2013, pp. 27–28, 104. DOI: 10.1137/1.9781611972702.

[13] Erik Cheever. *Fourth Order Runge-Kutta*. URL: https://lpsa.swarthmore.edu/NumInt/NumIntFourth.html.

A Path tracking details

Given a homotopy $H(t,x)$ and a solution to $x(1) = H(1,x)$, we numerically calculate the set of points $[x(t) : 0 \leq t \leq 1]$ such that $H(t,x(t)) = 0$ from $t = 1$ to $t = 0$. Since we have a point where $H(1,x(1)) = 0$, we want to find $x'(t)$ such that $H(t,x(t)) = 0$ is maintained. Differentiating $H(t,x(t)) = 0$ with respect to t gives us

$$H_x(t,x(t)) * x'(t) + H_t(t,x(t)) = 0 \tag{36}$$

and rearranging terms gives us

$$H_x(t,x(t)) * x'(t) = -H_t(t,x(t)). \tag{37}$$

We observe that $H_x(t,x(t))$ is the Jacobian of the system H with respect to x evaluated at time t. Left multiplying both sides of this equation by the inverse gives us

$$x'(t) = -H_x(t,x(t))^{-1} * H_t(t,x(t)). \tag{38}$$

We can now numerically integrate x with respect to t to calculate $x(0)$. One of the most popular methods for its accuracy and simplicity is the Fourth-Order Runge-Kutta predictor-corrector scheme [13], which states that given a function $f(t,\tilde{x})$ representing the derivative of x at point $\tilde{x}$ and time t, an approximation $\tilde{x}_t$ to x at time t, and time step Δt, we obtain an approximation for x at time $t - \Delta t$:

$$\tilde{x}_{t-\Delta t} = \tilde{x}_t + \frac{1}{6}(k_1 + 2k_2 + 2k_3 + k_4) \tag{39}$$

where

$$\begin{aligned}
k_1 &= \Delta t * f(t,\tilde{x}_t) \\
k_2 &= \Delta t * f(t - \frac{\Delta t}{2}, \tilde{x}_t + \frac{k_1}{2}) \\
k_3 &= \Delta t * f(t - \frac{\Delta t}{2}, \tilde{x}_t + \frac{k_2}{2}) \\
k_4 &= \Delta t * f(t - \Delta t, \tilde{x}_t + k_3)
\end{aligned}$$

In the above formulas, we can substitute in $f(t,\tilde{x}) = -H_x(t,\tilde{x})^{-1} * H_t(t,\tilde{x})$ to generate the approximation for $\tilde{x}$. This creates our **prediction** for $\tilde{x}_{t-\Delta t}$ given homotopy H, approximation $\tilde{x}_t$, time t, and time step $-\Delta t$.

This step moves in the direction of the path defined by (38), however, it might not stay on the path, i.e, $H(t,x(t)) = 0$ may not be satisfied. To refine our approximation so that $\tilde{x}_{t-\Delta t}$ stays on the path curve, we can repeatedly utilize Newton's operator:

$$N_F(x) = x - \left(\frac{\partial F}{\partial x}(x)\right)^{-1} F(x) \tag{40}$$

where $F(x) = H(t - \Delta t, x)$. As long as our approximation $\tilde{x}_{t-\Delta t}$ is, i.e, $\det(\frac{\partial F}{\partial x}(\tilde{x}_{t-\Delta t})) \neq 0$, Newton's method should converge quadratically and the accuracy of the approximation (measured by the number of accurate digits of said approximation) will double at each step [10]. This creates our **correction** for $\tilde{x}_{t-\Delta t}$ given homotopy H, current approximation $\tilde{x}_{t-\Delta t}$, and time $t - \Delta t$.

The fourth-order Runge-Kutta **predictor** and the Newton's method **corrector** above allow to numerically calculate the points on the path $[x(t) : 0 \leq t \leq 1]$ according to the algorithm below:

Algorithm 1: NaiveHomotopyTracking(H, x_1, N)

Result: This algorithm calculates $x(t)$ over N evenly spaced points over the interval $[0, 1]$ starting at known start solution x_1 and ending at target solution x_0 given a homotopy H that connects the start system and target system.

$\Delta t \leftarrow \frac{1}{N}$;

for $t = 1$ *to* Δt *with step* $-\Delta t$ **do**

  $k_1 = \Delta t * H(t, x_t)$;

  $k_2 = \Delta t * H(t - \frac{\Delta t}{2}, x_t + \frac{k_1}{2})$;

  $k_3 = \Delta t * H(t - \frac{\Delta t}{2}, x_t + \frac{k_2}{2})$;

  $k_4 = \Delta t * H(t - \Delta t, x_t + k_3)$;

  $x_{t-\Delta t} = x_t + \frac{1}{6}(k_1 + 2k_2 + 2k_3 + k_4)$;

  do

    $x_{t-\Delta t} = x_{t-\Delta t} - \left(\frac{\partial H}{\partial x}(t - \Delta t, x_{t-\Delta t})\right)^{-1} H(t - \Delta t, x_{t-\Delta t})$;

  while $|H(t - \Delta t, x_{t-\Delta t})| < 10^{-12}$;

end